

## ORIGINAL RESEARCH ARTICLE

# Spectral structure of surface waves and its influence on sediment dynamics

Boris V. Divinsky\*, Ruben D. Kosyan

*Shirshov Institute of Oceanology RAS, Moscow, Russia*

Received 9 April 2018; accepted 11 July 2018

Available online 28 August 2018

## KEYWORDS

Sand bottom dynamics;  
JONSWAP spectra;  
Acoustic backscatter  
measurements;  
Concentration profiles;  
Frequency domain

**Summary** Analysis of the influence of wave energy frequency distribution on the dynamics of suspension over the sea-bottom is the main objective of this study. We revealed the differences between the response of the eroded sea-bottom to external disturbances represented by irregular surface waves with permanent integral characteristics (significant wave height and frequency of the spectrum peak) and variable frequency of the wave energy distribution.

© 2018 Institute of Oceanology of the Polish Academy of Sciences. Production and hosting by Elsevier Sp. z o.o. This is an open access article under the CC BY-NC-ND license (<http://creativecommons.org/licenses/by-nc-nd/4.0/>).

## 1. Introduction

The dynamics of sea-bottom sediments plays an important role in the formation of foreshore morphological features. Many models exist for the analysis and the quantitative prognosis of sediment suspension and sediment transport by wave; these have been reviewed and compared by Davies et al. (2002). The hydrodynamic impact of waves (and cur-

rents) on the sea bottom is complex as in addition to the suspension of sediment from the bed there is also the impact on the sea-bed morphology via the formation and evolution of bed-forms. These bed-forms have the feedback on the hydrodynamics through bed friction and processes such as vortex ejection. In this paper, we use waves generated in a very large wave flume over a sandy bed to examine some of the processes and physical mechanisms important for the resuspension and transport of sand by waves.

Currents and wind-driven surface waves are very important for the sea-bottom sediment suspension and transport processes. The irregularity of waves is an important feature of wind-generated waves as irregular waves produce quite different patterns of suspension and bed-form dimensions from regular waves (Vincent and Hanes, 2002). Significant wave height and spectrum peak period are the main wave parameters. Generally, the surface wave spectrum can be described by the JONSWAP approximation, which is widely used in the engineering practice.

\* Corresponding author at: Shirshov Institute of Oceanology RAS, 117997, 36 Nahimovskiy pr., Moscow, Russia. Tel.: +7 918 4567922.

E-mail address: [divin@ocean.ru](mailto:divin@ocean.ru) (B.V. Divinsky).

Peer review under the responsibility of Institute of Oceanology of the Polish Academy of Sciences.



Production and hosting by Elsevier

<https://doi.org/10.1016/j.oceano.2018.07.003>

0078-3234/© 2018 Institute of Oceanology of the Polish Academy of Sciences. Production and hosting by Elsevier Sp. z o.o. This is an open access article under the CC BY-NC-ND license (<http://creativecommons.org/licenses/by-nc-nd/4.0/>).

The JONSWAP spectrum was developed in 1973 as a result of field observations in the North Sea (Hasselmann et al., 1973). It is presented in a general form as follows:

$$S(f) = \frac{\alpha g^2}{(2\pi)^4} f^{-5} \exp \left( -\frac{5}{4} \left( \frac{f}{f_m} \right)^{-4} \right) \gamma \exp \left( -\frac{1}{2\sigma^2} \left( \frac{f}{f_m} - 1 \right)^2 \right), \quad (1)$$

where  $f$  is the frequency,  $g$  is the acceleration of gravity,  $\alpha$  is the Philip's constant ( $\alpha = 0.0081$ ) and  $f_m$  is the spectrum maximum frequency.

The same spectrum is presented in the parameterized form:

$$S(f) = \beta h_s^2 f_m^4 f^{-5} \exp \left( -\frac{5}{4} \left( \frac{f}{f_m} \right)^{-4} \right) \gamma \exp \left( -\frac{1}{2\sigma^2} \left( \frac{f}{f_m} - 1 \right)^2 \right), \quad (2)$$

where  $\beta \approx \frac{0.0624}{0.230 + 0.0336\gamma - \left( \frac{0.185}{1.9 + \gamma} \right)}$ ,  $\gamma$  is the peak enhancement coefficient, and  $\sigma$  takes one of two values

$$\sigma_l \approx 0.07 \ (f \leq f_m) \ \text{or} \ \sigma_r \approx 0.09 \ (f > f_m). \quad (3)$$

Hence, the JONSWAP spectrum is determined by three main parameters: the significant wave height  $h_s$ , the spectrum peak frequency  $f_m$ , and the shape parameter  $\gamma$ . Generally,  $\gamma$  is taken to be equal to 3.3 in the sea-bottom sediment dynamics studies, which corresponds to the moderate wave formation conditions (Hasselmann et al., 1973).  $\gamma$  controls the spectrum form and characterizes to a great

extent the wave energy frequency distribution. The surface wave spectra and their JONSWAP approximations, obtained by Divinsky (2003) using a Datawell Waverider buoy in the Black Sea, are shown in Fig. 1 as illustrations of JONSWAP spectra with various shape parameters.

The use of formula (2) requires the specification of three parameters, two of which are known and determined from the experimental spectrum: the significant wave height  $h_s$  and the frequency of the maximum of the spectrum  $f_m$ . Setting the third parameter ( $\gamma$ ), we achieve the coincidence of the maxima of the spectra. In this case, the parameter that regulates the shape of the side lobes ( $\sigma$  in formula (2)) does not change.

In the spectra shown here (Fig. 2), the significant wave height is approximately 2.6 m, while the spectrum peak frequency is 0.15 Hz. However, although their spectral energy densities are almost equal there are considerable differences in the frequency distribution of the spectral energy. It is defined by the proportion of the wave energy concentration in the main peak of the irregular wave spectrum and is quantified by the  $\gamma$  parameter. Does this variation in wave irregularity significantly influence the suspension processes and the mobilization of sand from the sea-bed? An important objective of this work is to investigate the degree to which the suspension processes and sea-bottom matter redistribution are affected by irregularity of the surface waves with constant integral characteristics (the same values of significant wave height and spectrum peak frequency) and variable frequency distribution of the spectral wave energy (variable value of parameter  $\gamma$ ).

The influence of the surface waves spectral structure on bottom sediment suspension was earlier addressed in the SISTEX99 experiments (Dohmen-Janssen et al., 2000; Vincent

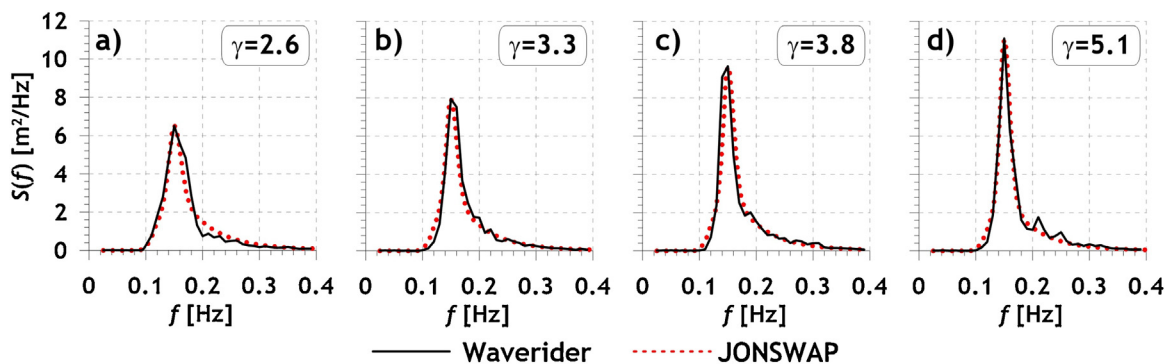


Figure 1 Wind-driven wave experimental spectra and their approximations by the JONSWAP spectrum.

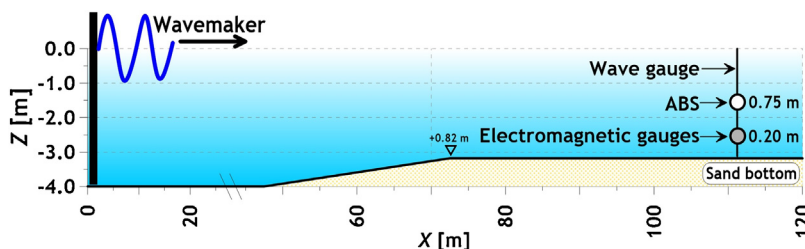


Figure 2 Scheme of the experiment.

and Hanes, 2002) using monochromatic waves, waves with a pronounced group structure, and random waves. The main conclusions of these studies concerned the dependence of the characteristics of suspension on the intensity of the waves, characterized by the height of the waves.

In our case study, we analyse a series of observations carried out at constant wave heights (and periods) under conditions of a wave spectral composition transformation which are the continuation of a previous work presented in Grüne et al. (2007) and Kos'yan et al. (2010).

In 2014, a paper was published (Divinsky et al., 2014). Both works (2014 and the present), based on the same experimental data, share a common goal, namely the study of the effect of the spectral composition of the wave on the regularities of suspension. However, these two studies set completely different objectives. The paper of 2014 focused on the dynamics of bottom-microforms (ripples). In this paper: (1) physical conditions and techniques of the experiment are described in detail (in 2014 this was not possible due to limitations on the format of the article); (2) important issues of data processing and interpretation are discussed; (3) the influence of the surface waves spectral structure on the redistribution of the bottom material is investigated; (4) the features of suspension in the frequency domain are analyzed. Thus, the present work can be considered as a further step in the study of the sand suspension regularities under the conditions of real irregular surface waves.

## 2. Material and methods

### 2.1. Experimental conditions

Experiments were conducted in 2008, led by Russian and German scientists, in the Large Wave Channel (LWC) of the Coastal Research Centre in Hannover, Germany. They included setting-up the laboratory channel and the control and production of the external hydrodynamic environment parameters to provide the specific laboratory wave conditions.

The LWC is the biggest wave channel in Europe and can be used for prototype-scale engineering and scientific experiments to study the shoreline dynamic processes. The LWC is 307 m long, 5 m wide, with 7 m high sides. Depending on the waves being produced and the depth of the sediment in the channel, this limits the maximum water depth to around 5 m. Surface waves with given statistical and spectral properties are generated by a program-controlled segmented paddle at one end of the channel. The LWC was equipped with string wave recorders located at known distances from the wave generator. At the far end of the channel, waves are absorbed by a sandy beach or a series of absorbing grids. In the course of these experiments, the bottom of the LWC was covered with a sand layer ~0.8 m thick; the median sand particle size  $d_{50}$  was 0.225 mm. Our measuring instruments were set at a distance of 111.45 m from the wave generator, at an initial still-water depth of 3.18 m (Fig. 2) close to the location of one of the LWC string wave recorders, which recorded water level at 40 Hz.

The two used instruments were: (1) an Aquascat 1000 multi-frequency profiling acoustic backscattering system (ABS) which was installed with the acoustic sensors 'looking' vertically downwards at a distance of 0.75 m from the initial sand bed and (2) a Stromungssensor Type S

electromagnetic velocity meter mounted at 0.2 m from the initial bed which was used for measuring the longitudinal  $U$  and transverse  $V$  components of the water flow velocity. The ABS operating frequencies were 1, 2 and 3.84 MHz.

### 2.2. The processing of ABS data

The task is to determine the time-series of the profiles of suspended sediment mass concentration from the backscattered acoustic signal power from the ABS sensors (Thorne et al., 1991; Thorne and Hanes, 2002). The backscattered voltage  $V_{rms}$  measured by an ABS transducer from a mass concentration of scatterers  $M$  at a distance  $r$  from the transducer can be described by

$$V_{rms} = \frac{k_s k_t}{\psi r} M^{1/2} e^{-2r(\alpha_w + \alpha_s)}, \quad (4)$$

where

$$k_s = \frac{\langle f \rangle}{\sqrt{\langle a_s \rangle} \rho_s} \quad (5)$$

and

$$\alpha_s = \frac{3}{4r\rho_s} \int_0^r \frac{\langle \chi \rangle M}{\langle a \rangle} dr. \quad (6)$$

Here,  $k_t$  is the system calibration factor,  $\langle a_s \rangle$  is the mean particle size,  $\rho_s$  is the density of sediment,  $\alpha_w$  is the attenuation due to absorption by sound in the water column,  $\alpha_s$  is absorption due to the presence of the sediment,  $\psi$  is a correction factor. The most important acoustic terms in Eqs. (5) and (6) are the two functions:  $\langle f \rangle$ , describing the scattering power of suspended particles, and  $\langle \chi \rangle$  which determines the nature of the passage and attenuation of the acoustic signal in the water column in the presence of suspended solids.

Using Eq. (4) with known scattering properties of the medium it is possible to build a vertical power profile of the backscattered signal. The inverse task is to use Eq. (4) to determine the mass concentration of suspended sediment. When using a single frequency ABS to determine the concentration of suspended solids there is a need for repeated determination of the granulometric composition of suspended matter. In most wave-dominated environments, the mean size of the particles and concentration of particles in suspension have complex spatial-temporal variations. External dynamic effects (currents, wave motion, turbulence, gravity) create a spatially inhomogeneous field (gradient) of suspended particles. On this basis, the measurement results were processed by the implicit method involving data from all three working frequencies.

In the case of multiple ABS operating at different frequencies, in addition to the concentration profile of suspended sediment it is possible to estimate the profile of the mean size of the particles: the mean diameter of the particles is taken from the sediment diameter which minimizes the differences between the concentrations values of suspended solids (Thorne and Meral, 2008).

The multi-frequency acoustic signals from a suspension are converted, using Eqs. (4)–(6), into values of suspended sediment concentrations  $M$  and the mean particle size  $\langle a \rangle$ . Expressions for  $\langle f \rangle$  and  $\langle \chi \rangle$ , included in Eqs. (5) and (6), have the form (Thorne and Meral, 2008):

$$\langle f(x_0) \rangle = \left( \frac{\int_0^\infty aP(a)da \cdot \int_0^\infty a^2 f(x)^2 P(a)da}{\int_0^\infty a^3 P(a)da} \right)^{1/2}, \tag{7}$$

$$\langle \chi(x_0) \rangle = \frac{\int_0^\infty aP(a)da \cdot \int_0^\infty a^2 \chi(x)P(a)da}{\int_0^\infty a^3 P(a)da}, \tag{8}$$

$$\langle a \rangle = \int_0^\infty aP(a)da,$$

where  $a$  is the radius of the sand particles,  $P(a)$  is the distribution function of suspended particle sizes,  $x = ka$ ,  $k$  is the wave number ( $k = 2\pi/\lambda$ ,  $\lambda$  – length of acoustic wave),  $x_0 = k\langle a \rangle$ .

To determine the suspended particles concentration from Eqs. (7) and (8), which is required, the assignment functions  $f$  and  $\chi$  should be accordingly defined. In the paper Thorne and Meral (2008) empirical approximations, based on the analysis of numerous data from field observations, have been proposed. For the functions  $f$  and  $\chi$  they have the form:

$$f = \frac{x^2(1 - d_1 5e^{-(x-d_2)/d_3})^2(1 + d_4 e^{-(x-d_5)/d_6})^2(1 + d_7 e^{-(x-d_8)/d_9})^2}{d_{10} + d_{11}x^2}, \tag{9}$$

$$\chi = \frac{c_1 x^4}{c_2 + c_3 x^2 + c_4 x^4}. \tag{10}$$

The coefficients  $c_n$  and  $d_n$ , included in Eqs. (9) and (10), were determined experimentally for a real sandy bottom (Thorne and Meral, 2008). Moate and Thorne (2011) studied the acoustic scattering properties of typical marine sediments materials (quartz, rakusa, aragonite, mica, olivine, zircon, and magnetite) and for each material identified the coefficients  $c_n$  and  $d_n$ . A conclusion about significant differences in the behavior of the dispersion functions, and the necessity of taking into account the mineralogical composition of suspended matter was made.

In order to establish the distribution function of sand particle sizes, which is included in Eqs. (7) and (8), a grain size composition analysis was performed on the sediments forming the bottom of the experimental channel. Fig. 3 shows the graphs of the probability density and distribution function of particle sizes of sand. The size histogram is shown at the top of Fig. 3, and the percentage exceedance distribution is shown below; experimental data are in red. The blue curves show a lognormal distribution fitted to the data, indicating the bottom sediments conform approximately to a lognormal distribution (Kolmogorov–Smirnov test = 0.096,  $p < 0.01$ , Chi-square test = 93.51). In this case, the median sand

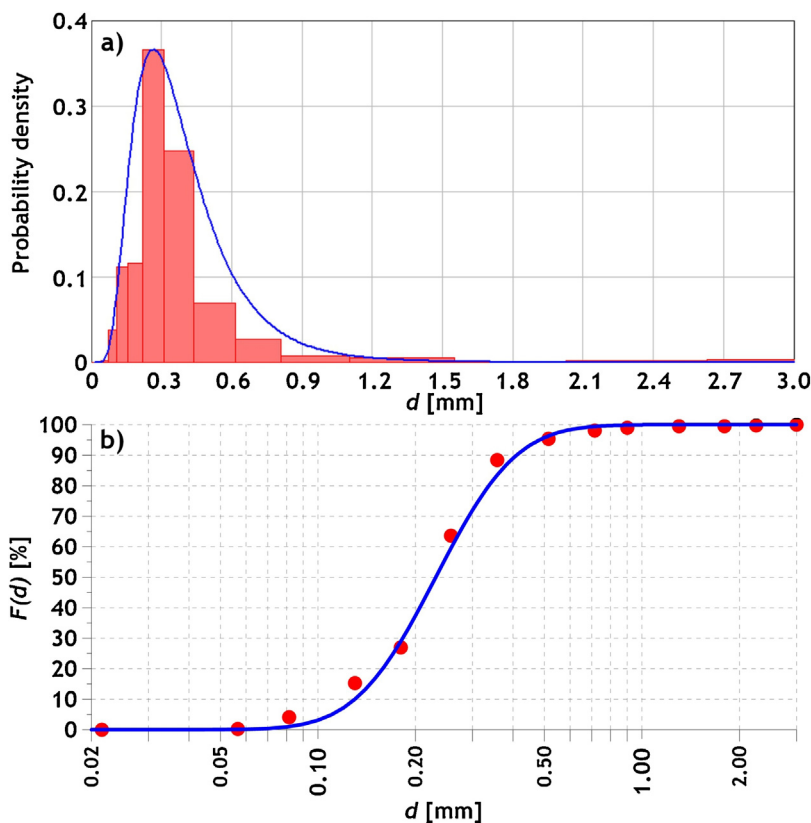


**Figure 3** The probability density (a) and distribution function (b) of sand particle sizes. The blue line is an approximation to the lognormal distribution law.

**Table 1** Characteristics of acoustic emitters.

Frequency, MHz	1.00	2.00	3.84
The radius of the emitter [mm]	9.00	4.80	4.85
The system calibration factor $k_t$	0.02259	0.00915	0.00880

particle size  $d_{50}$  is equal to 0.225 mm, with a  $\sigma_d$  geometric standard deviation, defined as  $(d_{84}/d_{16})^{0.5}$ , of 0.338 mm.

The lognormal distribution function  $F(d)$  is a function in the form of:

$$F(d) = 0.5 \left[ 1 + \operatorname{erf} \left( \frac{\log(d/d_{50})}{\sqrt{2} \log \sigma_d} \right) \right], \quad (11)$$

where  $\operatorname{erf}$  is the error function.

In summary, the processing of the acoustic signals, scattered by suspended sand particles, is as follows:

1. The bottom is a layer of quartz river sand with a median particle size  $d_{50}$  equal to 0.225 mm and a standard deviation of 0.338. The distribution of particle size corresponds to the lognormal one with the distribution function in the form of Eq. (11).
2. The characteristics of the acoustic transmitters are given in Table 1.
3. The function  $\langle f \rangle$ , describing the scattering power of suspended particles, and  $\langle \chi \rangle$ , responsible for the nature of the passage and attenuation of the acoustic signal in the water column in the presence of suspended particles, are approximated by using expressions (9) and (10), respectively.

### 2.3. Experimental data

Sequences of the free surface waves, described by a JONSWAP spectrum, were generated in the LWC, with characteristics described below, and random phases. The investigated experimental conditions correspond to the following set of spectral parameters of the initial wave field:

- significant wave height  $h_s = 0.8, 1.0, 1.2$  m;

- spectrum peak frequency  $f_m = 0.2$  Hz;
- peak enhancement parameter  $\gamma = 1.0, 1.5, 2.0, 2.5, 3.0, 3.3, 4.0, 6.0, 8.0, 9.9$ ,

making a total of 30 wave sequences of irregular surface waves (each series duration was about 33 min). Suspended sediments concentrations were measured using the ABS for each sequence.

The ABS data processing resulted in the generation of time series data of suspended sand concentrations and mean grain diameters in the water column, as well as in the detection of the local sand bed surface location based on the sharp intensification of the sonar echoes records. Examples of the processed ABS data are given in Figs. 4–6. The time interval between profiles is 0.25 s, and the vertical spatial resolution is 1 cm. The figures show the mean diameter of the sand grains, the concentrations of the suspended sediments, and the free surface elevations. The periods of suspension and redistribution of the sand from the bed are clearly seen, both at the scale of single waves and for wave packets (groups).

Before proceeding to the discussion of the results, we wish to emphasize the following important points.

First, although the reconstruction of the suspended sediment concentration profiles and the mean sand grains diameters from the analysis of the acoustic power of the multi-frequency ABS echo signals is not a trivial task, the main objective of this paper is to estimate the influence of the peak enhancement factor of the surface wave spectral structure on the sea-bottom sediments dynamics. We assume that the errors of measuring and interpretation of the acoustic signals in all observation series are the same.

Second, the shape of the JONSWAP wind-driven wave spectra approximation is determined by the  $\gamma$  and  $\sigma$  parameters in Eqs. (1) and (2). Parameter  $\sigma$  specifies the shape JONSWAP spectrum on either side of the spectral peak ( $\sigma_l$  defines the shape of the low-frequency part of the spectrum while  $\sigma_r$  defines the high-frequency part). The values of  $\sigma$ , in Eq. (3) as shown in Hasselmann et al. (1973), are estimated when the peak  $\gamma$  parameter value is equal to 3.3. The work represents a sufficient approximation for the other values of  $\gamma$  obtained when the  $\sigma$ -parameter is equal to the other values. In this case, Hasselmann's values for  $\sigma$ ,  $\sigma_l = 0.07$  and  $\sigma_r = 0.09$ , were used for all  $\gamma$  values. The forms of the

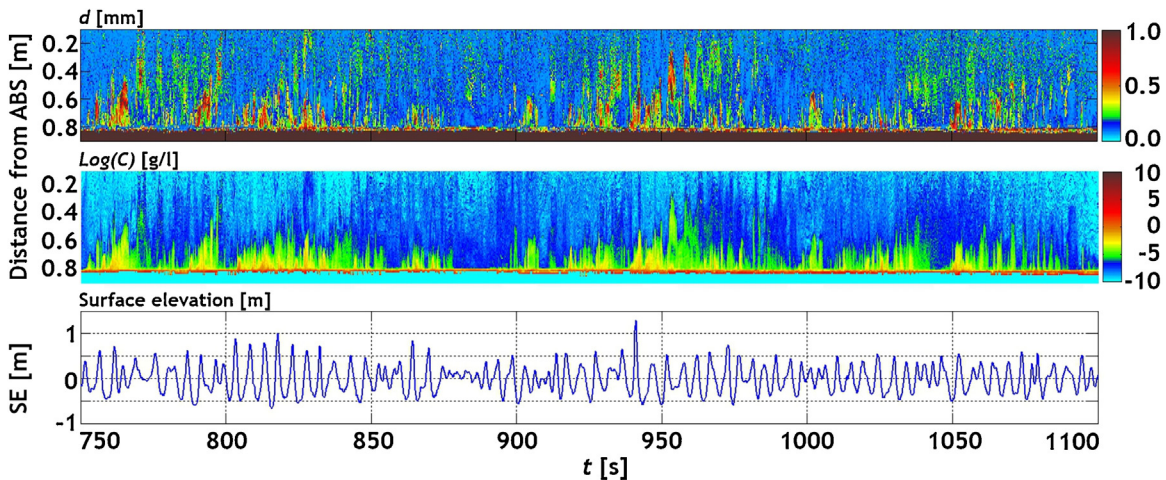


**Figure 4** From top to bottom: distribution of the mean diameters of sand particles, concentrations of suspended sediments, and free surface elevation in the experiments with the following parameters:  $h_s = 1.2$  m,  $f_m = 0.2$  Hz,  $\gamma = 2.5$ .

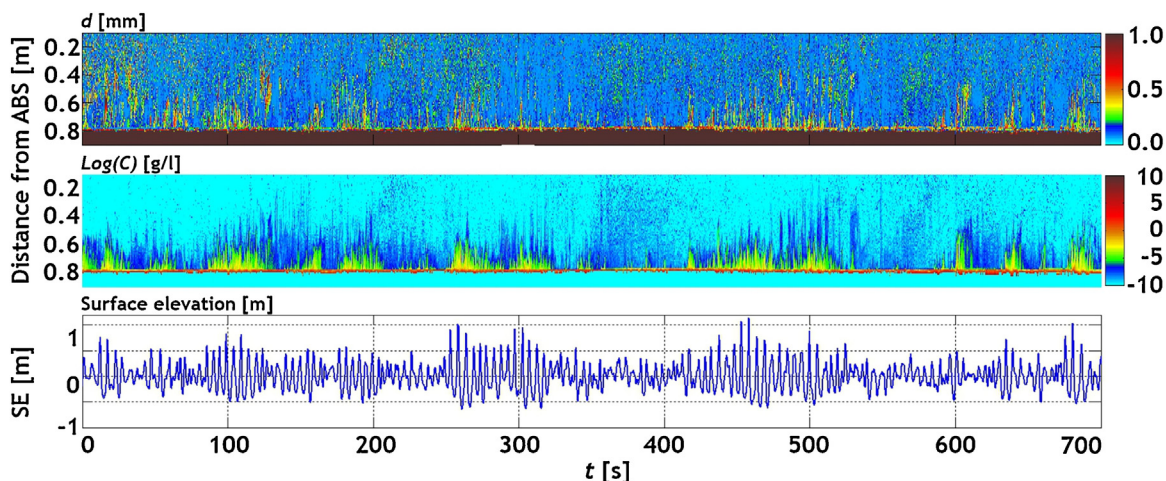


**Figure 5** From top to bottom: distribution of the mean diameters of sand particles, concentrations of suspended sediments, and free surface elevation in the experiments with the following parameters:  $h_s = 1.0$  m,  $f_m = 0.2$  Hz,  $\gamma = 6.0$ .

JONSWAP spectra represented in Fig. 1, were obtained using these values. The same constants ( $\sigma_l$  and  $\sigma_r$ ) were specified in the experimental generation of the free surface elevation series by the wave generator. We believe that this assumption of constant  $\sigma$  does not have a strong influence on the final results.

Third, the JONSWAP parameterisation is available only for a spectrum with a dominant single-peak. Transformations in the wave spectrum can be a result of bottom friction, wave breaking, or non-linear wave interactions. We estimated the variation in the  $\gamma$  parameter of our surface waves along the LWC from the generation region to the observation point. An example of the parameter  $\gamma$  transformation for the case of  $h_s = 1.2$  m,  $f_m = 0.2$  Hz is shown in Fig. 7.

The data used in our estimates were obtained using string wave recorders located along the LWC generator. The  $\gamma$  parameters were determined at the points located at the distances of 50, 79, 102, and 111 m from the wave generator. Fig. 7 shows how  $\gamma$  changes along the channel; the initial  $\gamma$  is defined as the value at the wave generator, indicated by the

$\gamma_{\text{Wavemaker}}$  values on the left of Fig. 7. Table 2 shows the measured  $\gamma$ .

The results show a strong transformation of the surface wave spectra, associated with the wave profile transformation and partial dissipation of the wave energy, which takes place as the significant wave height increases.

The wave energy transfer is observed from the region of the main maximum together with the flattening of the spectrum, which is associated with a decrease in the  $\gamma$  parameter. The spectral densities of surface waves at the location of the ABS (111.45 m from the wave generator) generally differ from the initial spectral densities. Analysis of waves at the location of ABS shows that for all series of observations the frequency of the maximum of the spectrum is unchanged (0.2 Hz) while the significant wave heights varied within the range of 5–6% (Table 3).

The data in Tables 2 and 3 show that surface waves in the LWC propagate practically without loss of energy and the rearrangement of the wave field is related to the interaction between the spectral components, which makes it possible to

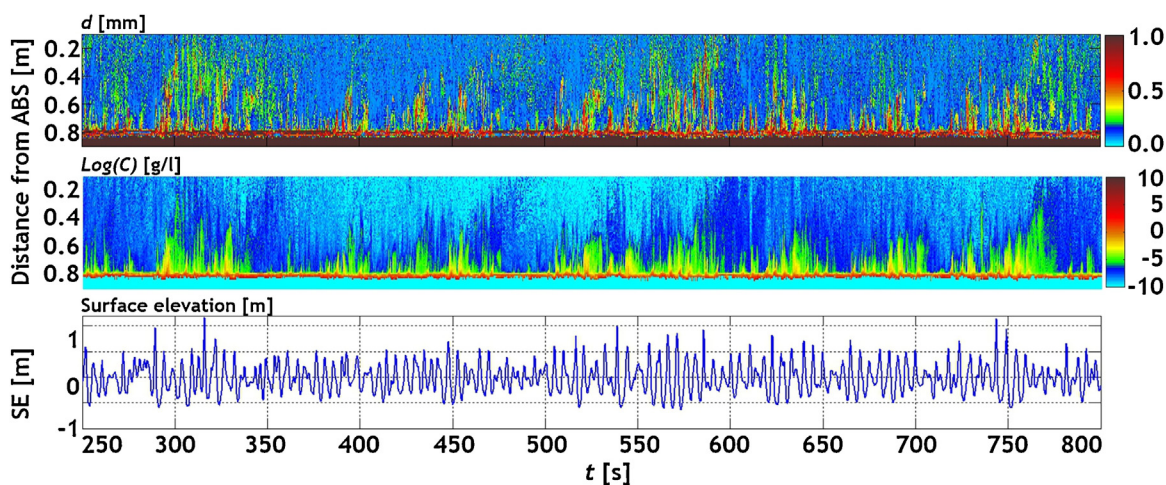


**Figure 6** From top to bottom: distribution of the mean diameters of sand particles, concentrations of suspended sediments, and free surface elevation in the experiments with the following parameters:  $h_s = 1.2$  m,  $f_m = 0.2$  Hz,  $\gamma = 4.0$ .

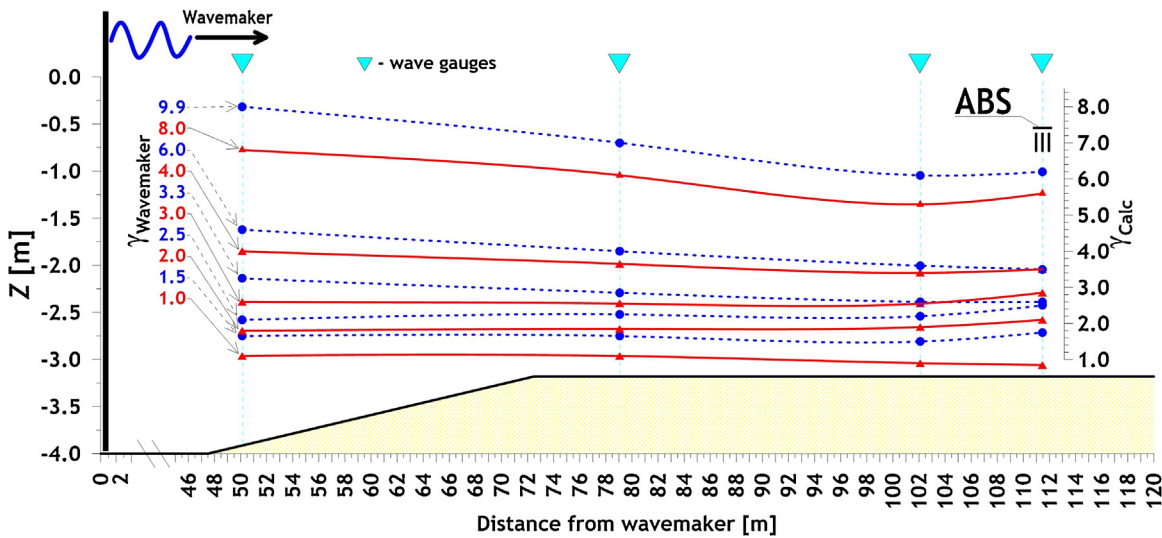


Figure 7 Variation in the  $\gamma$  parameter related to the propagation of waves in the experimental channel ( $h_s = 1.2$  m).

analyze the influence of the features of spectral structure of the surface wave on the regularities of suspension of bottom material.

Furthermore, a few important remarks should be made. The effect of irregular surface waves on sediment is the formation of a characteristic profile of the bottom. The profile structure is defined by the balance between the hydrodynamic forces acting in the flow and the characteristics of the bottom material. In our laboratory experiment, the amount of material constituting the bottom remains constant, although the sand may be redistributed along the channel profile.

A mathematical model was developed to simulate and thus clarify the mechanisms controlling the redistribution of bottom material in the wave channel by irregular waves. It is phase-resolving, based on the numerical solution of the Boussinesq equations, and describes the behavior of individual waves as they propagate along the channel. The geometry of the computational channel fully corresponds to the Hannover Large Wave Channel: with length 300 m, width 5 m, smooth vertical walls, a horizontal layer of sand with a thickness of 0.82 m with an up-wave slope of 1:25, and water depth of 4 m. The surface waves in the model corresponded to those measured over a 20-min time period close to the wave-generator and had the following integral parameters of the JONSWAP spectrum: significant wave height  $h_s = 1.0$  m, peak frequency of the spectrum of  $f_m = 0.2$  Hz,  $\gamma = 3.3$ .

The simulation result is shown in Fig. 8. The software wave maker, generating a number of elevations of the free surface, was located at the position of 10 m in the x-axis. The figure shows:

- (a) the instantaneous elevation of the free surface;
- (b) the component of the wave energy in the direction of wave propagation  $P$ ;
- (c) the transverse component of wave energy  $Q$ ;
- (d) the underwater profile of the channel, including areas of hard bottom and sand layer.

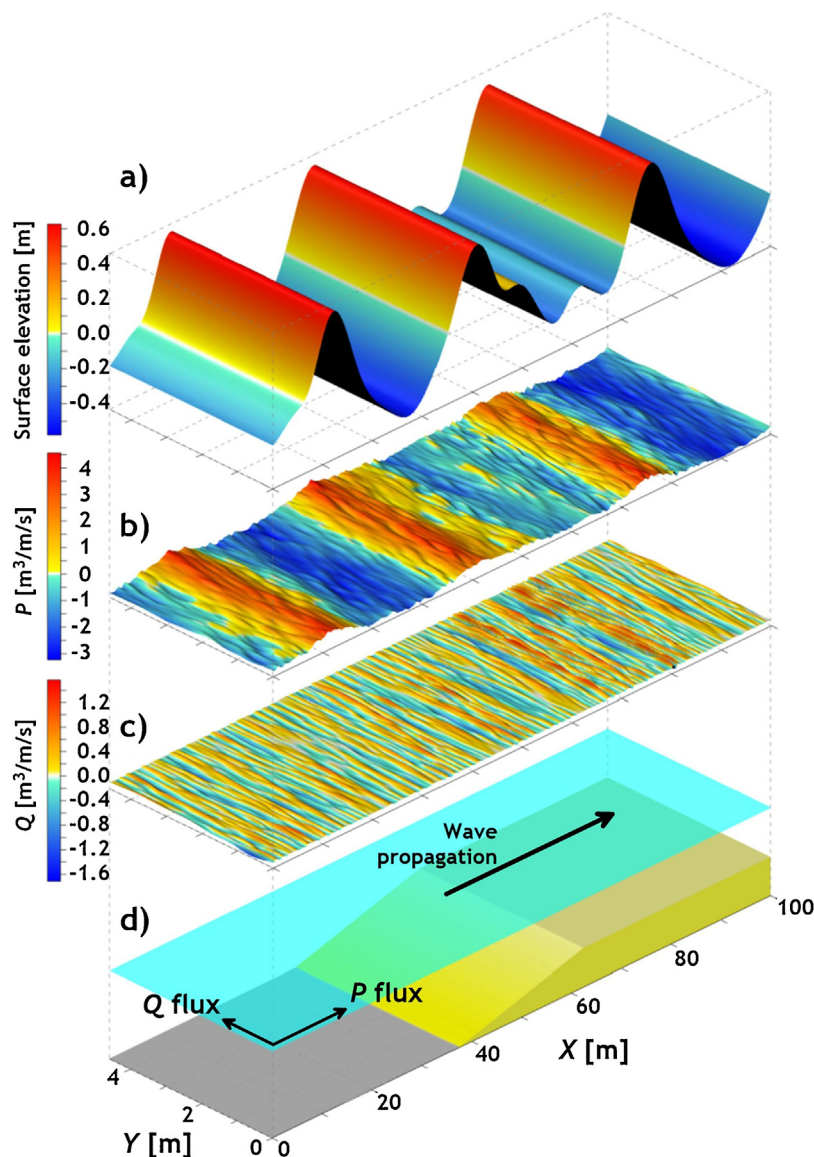
As can be seen from Fig. 8, the horizontal heterogeneity of the irregular wave flow lies in the fact that the wave action vector randomly deviates from the longitudinal axis of the channel. The proportion of wave energy transmitted in the transverse direction can reach 15–20% of the total wave energy. Such horizontal heterogeneity is caused by the interaction of waves with the bottom and with the channel walls. Ultimately, the process of formation of zones of erosion or accumulation of bottom material becomes essentially random. In addition, during the generation of irregular surface wave, the initial phase is set at random. The randomness of the initial phase of the waves determines the randomness of the sequence of elevations of the free surface and, as a result, the coincidence effect.

Table 2 Initial  $\gamma_{\text{Wavemaker}}$  and calculated  $\gamma_{\text{Calc}}$  values of the JONSWAP enhancement factor.

$h_s$ [m]	$\gamma_{\text{Wavemaker}}$									
	1.0	1.5	2.0	2.5	3.0	3.3	4.0	6.0	8.0	9.9
	$\gamma_{\text{Calc}}$									
0.8	1.02	1.34	1.71	2.37		3.04	3.41	5.15	6.68	7.57
1.0	1.13	1.85	2.12	2.55	2.89	2.67	3.91	3.95	6.51	7.61
1.2	0.85	1.75	2.11	2.51	2.85	2.60	3.47	3.51	5.60	6.20

Table 3 Significant wave heights at the observation point.

$h_s$ [m]	$\gamma_{\text{Wavemaker}}$									
	1.0	1.5	2.0	2.5	3.0	3.3	4.0	6.0	8.0	9.9
	$h_s$ in point of measurements [m] (111.45 m from wave generator)									
0.8	0.80	0.78	0.80	0.80	0.81	0.79	0.76	0.82	0.82	0.82
1.0	0.98	1.01	0.99	1.02	1.01	0.99	1.04	1.02	1.06	1.06
1.2	1.18	1.18	1.15	1.17	1.17	1.17	1.21	1.20	1.23	1.25



**Figure 8** One-dimensional irregular waves propagation in a wave channel: (a) the elevation of the free surface, m; (b)  $P$ -component of the horizontal wave energy flux,  $\text{m}^3/\text{s}/\text{m}$ ; (c)  $Q$ -component of horizontal wave energy flux,  $\text{m}^3/\text{s}/\text{m}$ ; (d) the schematic presentation of the bottom profile.

### 3. Discussion

#### 3.1. Sea-bed dynamics

Acoustic transducers make possible detecting the location of the hard sea bottom, which is determined as the point on the vertical profile with sharp echo signal intensification. On the profiles, this is clearly for the pair of adjacent points at which measurements have been performed and within a short distance of the spatial discreteness of the measurements (1 cm): the sediment concentrations at the point lying below are 10–20 times higher than the concentrations in the neighboring point located 1 cm above. The vertical coordinate for the point with a high concentration is taken as the position of the solid bottom.

The transformation of the sea bottom during the experiment is shown in Fig. 9. Note that Fig. 9 illustrates also the stages of

the whole experiment; for this reason, the enhancement factor is indicated in the form of the initial value  $\gamma_{\text{Wavemaker}}$ .

The data used to plot Fig. 9 were smoothed by a low-frequency filter to demonstrate the general trend in the depth variation under the acoustic transducers. According to the conditions of the experiment, the 30-min consecutive observation series correspond to the specified initial spectral parameters of the surface wave ( $\gamma_{\text{Wavemaker}} = 1$ ,  $h_s = 0.8$  m), ( $\gamma_{\text{Wavemaker}} = 1$ ,  $h_s = 1.0$  m), ( $\gamma_{\text{Wavemaker}} = 1$ ,  $h_s = 1.2$  m), ( $\gamma_{\text{Wavemaker}} = 1.5$ ,  $h_s = 0.8$  m), ( $\gamma_{\text{Wavemaker}} = 1.5$ ,  $h_s = 1.0$  m),  $\dots$ , ( $\gamma_{\text{Wavemaker}} = 9.9$ ,  $h_s = 1.2$  m). Usually, sea-bottom fluctuations were smaller than 2–3 cm during the period of each series. Nevertheless, an increase in the deformation of one sign (erosion or accumulation) indicates that significant potential sea-bed displacements are possible.

Fig. 9 is based on the data obtained from a 3.84 MHz transducer. The existing operational frequencies of the device

(1, 2 and 3.84 MHz) interact differently with suspended and organic matters, bubbles, or sea-bottom sediment layers. The conditions of each experiment are unique so that optimal results on the concentration profiles can be obtained from the comparison of the data received using individual frequencies or averaging different frequencies, for example, 2 and

3.84 MHz. All three frequencies are used to obtain the profile of the particle mean sizes, because, in this case, the minimum dispersion of the scattered signal is important.

The irregularity of accumulation processes together with sea-bottom matter erosion are the consequences of the surface wave influence on the eroded seabed. For example,

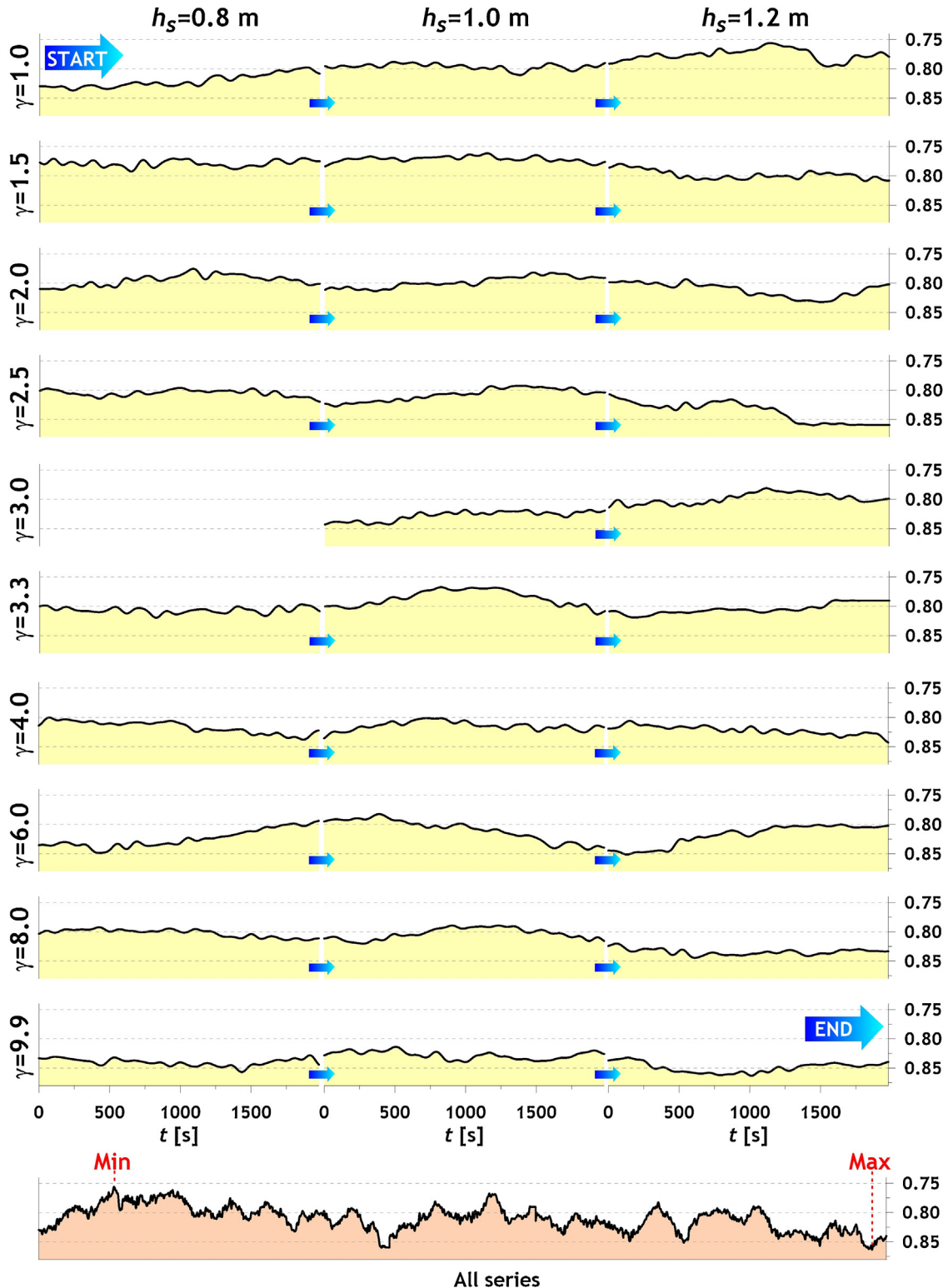


Figure 9 Location of the sand-bottom based on the results of individual sequential observation series.

according to Fig. 9, the experimental set with parameters [ $h_s = 0.8$  m,  $\gamma_{\text{Wavemaker}} = 6.0$ ] is characterized by substantially permanent sand accumulation at the point of observation; erosion consistently dominates in the conditions of parameters [ $h_s = 1.0$  m,  $\gamma_{\text{Wavemaker}} = 6.0$ ]; while permanent alteration of the sea-bottom deformation mark takes place in the case of the set of parameters [ $h_s = 1.0$  m,  $\gamma_{\text{Wavemaker}} = 4.0$ ]. At the same time, statistical data processing allowed us to reveal regularities in the sea-bottom configuration variations.

The statistical values of the estimates of the sea bottom location depend on the parameters of the initial wave field (mean, 25% and 75% quintiles, minimum, and maximum) shown in Fig. 10.

It should be highlighted that the results shown in Fig. 10 were obtained not for single measurements of the position of the solid bottom, but they are the statistical processing of thirty experimental series of observations. The duration of each series is 1980s (~33 min), the discreteness is 0.25 s. Even though that at any given moment under the ABS sensors there can be one or another feature of the microrelief, the averaging of the observational data makes it possible to estimate the average character of the surface waves effect on the eroded bottom. In addition, taking into account the surface waves transformation along the path from the point of the wave generation, the results are given in dependence on the parameters calculated at the ABS setting point enhancement factors.

As it follows from Fig. 10, the statistical characteristics of the solid bottom position for each series of experiments undergo considerable fluctuations. This is indicated by the interquartile range and the position of the minima and maxima. Nevertheless, the mean values have an obvious tendency indicating an increase in the local depth with the increase in the enhancement factor.

Thus, there is a reason to believe that this conclusion is based on (the gain of washout) location-specific observations. Instead of the conclusion about the strengthening of the local erosion of the values of the parameter  $\gamma$ , it would be probably correct to point out to a noticeable trend of an increasing impact on a sandy bottom with the parameter  $\gamma$  growth. The summary conclusion would be: the obtained result (shown in Fig. 8) clearly indicates a possible influence of the shape of the spectrum of the irregular surface waves on the dynamics of sediments.

### 3.2. Vertical profiles of the suspended particle concentrations and mean sizes

We estimated how important were the differences in the vertical distributions of the suspended particles when a sur-

face wave propagated over an eroded sea bottom. The profiles of the suspended particle concentrations and the profiles of the mean sand sizes for the observation sets at  $h_s = 1.2$  m,  $f_m = 0.2$  Hz, and the variable  $\gamma$  parameter are shown in Fig. 11.

Actually, the near-bottom averaging is not informative because the transformation of the sea-bottom profile is very strong (Fig. 9). Correspondingly, the region in Fig. 11 with light brown colour generally shows the sea-bottom. It is seen from Fig. 11 that the vertically suspended particle field becomes more homogeneous as the  $\gamma$  parameter increases. The decrease in the mean particle diameters vertically is related to the low  $\gamma$  value. The grain-size composition does not change strongly above the sea bottom when the peak parameter increases. Large values of the mean diameter in the erosion layer may appear owing to the influence of the physical factors (erosion of light fraction) as well as due to the uncertainties in the interpretation of the reflections of the acoustic signal.

Microforms of the bottom topography may be shaped depending on the condition of the sea bottom and the dynamic characteristics of the water flow. These microforms in their turn affect the suspension processes and the vertical redistribution of the sea-bed material. The size of the vortices becomes larger as the linear size of the ripples increases. This facilitates sand transport in the vertical direction. The geometric size of ripples strongly influences the general process of suspension. Further, we investigate whether the  $\gamma$  parameter increase affects the ripple characteristics.

### 3.3. Regularities of the bottom sediments suspension in the frequency domain

As a result of the experiment, synchronous time series of suspended sediment concentrations and water flow velocity were obtained, which makes it possible to evaluate their interrelations in the frequency domain. The bottom series of concentrations have been selected corresponding to a level of 0.03 m from the current bottom. The speed sensor, recall, has been located at a distance of 0.20 m from the bottom.

It is worth emphasizing that an important condition for the purity of the experiment is, of course, the idle run of the wave with the specified characteristics, at which the bottom surface is adjusted to new hydrodynamic conditions. After that, the recording of the parameters of interest begins. Preliminary estimates showed that in this particular case, the truncation of the existing 33-min records (for example, 20 min for overlocking, 13 min for analysis) did not signifi-

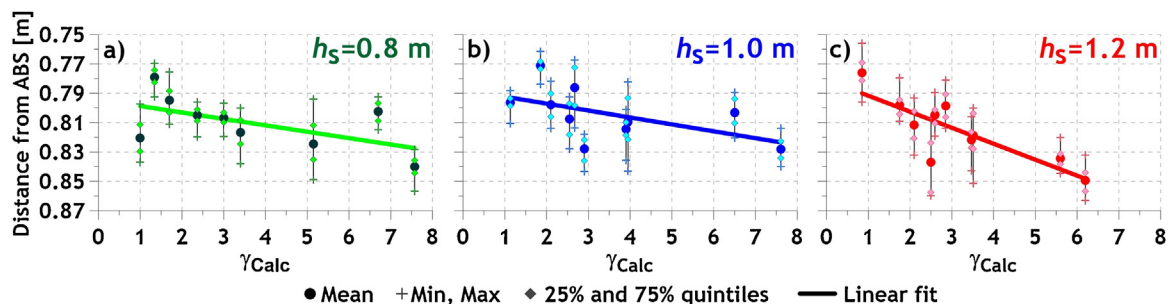


Figure 10 Statistical characteristics of the sand bottom location in the different observation series.

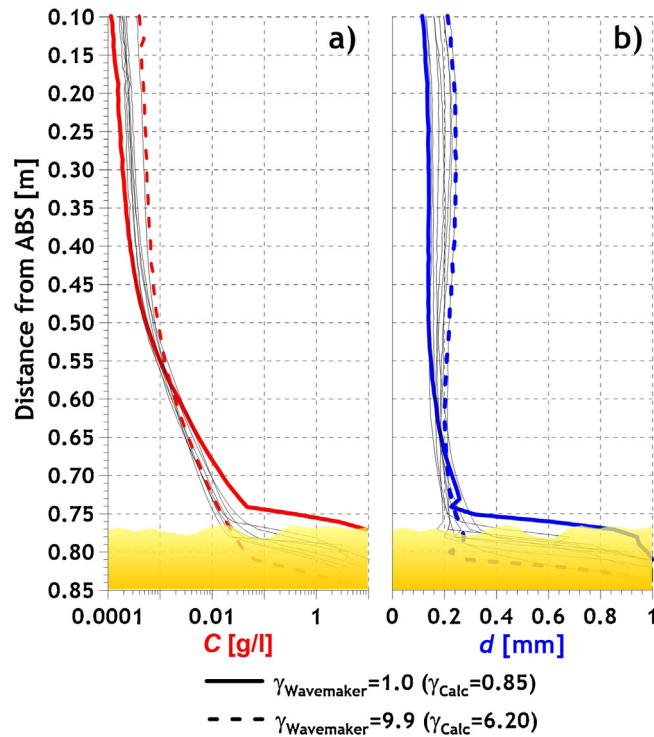


Figure 11 Vertical profiles of concentration (a) and mean diameter of suspended particles (b).

cantly affect the final results, so we used the full-length records (1980s) in further estimates.

To identify the features associated with the time structure of the velocity and concentration series, we applied the well-known Welch method. All further calculations using the periodogram method of Welch spectral analysis were carried out in the Matlab environment.

We should point out two characteristic features of the Welch method:

- use of the weighting function. It largely prevents the spreading of the spectrum and reduces the bias of the obtained assessment of the spectral components at the cost of a slight deterioration in the resolving power;
- splitting the signal into overlapping fragments. It allows increasing the total number of segments and thus reduces the variance of the estimate.

To study the frequency structure of the relationship between the velocity and concentration oscillations, we used the function of the mutual spectral density, namely the cospectrum, i.e. the real part of the cross-periodogram  $Co(f)$ . Cospectrum is a measure of the correlation of the same phase frequency components of two time series and is, therefore, a measure of the mutual energy of synchronous oscillations.

An example of processing of the velocity and concentration rows for the experimental series with initial parameters ( $h_s = 1.2$  m,  $f_m = 0.2$  Hz,  $\gamma = 8.0$ ) is given in Fig. 12.

The distribution of the spectral density of fluctuations of the normal to shore component of the near-bottom water velocity  $S_U$  is characterized by the presence of two peaks: the main peak at 0.2 Hz and the low frequency peak (0.031 Hz) associated with the group structure of waves (Fig. 12a).

Three local maxima clearly appear in the  $S_{SSC}$  concentration spectrum (Fig. 12b): at the fundamental frequency of the peak of the wave spectrum (0.2 Hz), its doubled frequency (0.4 Hz), since the sediment suspension occurs twice during the wave period, and also the low-frequency (0.031 Hz). The maximum energy of synchronous fluctuations in water velocity and concentration is collected at two frequencies: 0.2 Hz and 0.031 Hz (Fig. 12c).

The sign of the cospectrum indicates the direction of transfer of the bottom material. In our case, in almost the whole range of variability, sand moves from the shore.

For further analysis (and comparison) of the suspension features under different initial conditions, we defined some parameters characterizing the energy properties of the processes:

- Energies of low  $E_U(\text{low})$ ,  $E_{SSC}(\text{low})$  and high-frequency  $E_U(\text{high})$ ,  $E_{SSC}(\text{high})$  oscillations of water velocity and concentrations (Fig. 12a, b). The division of the spectrum into low- and high-frequency components is made from the velocity spectrum. In the example shown in Fig. 12 the separating frequency is 0.1 Hz. The energy of high-frequency  $E_{SSC}(\text{high})$  concentration fluctuations includes the entire range from the separation frequency, since the spectral peak at the doubled frequency of the maximum is not clearly visible for all series of observations;
- the magnitudes of the cospectra (Fig. 12c) are corresponding to two frequencies: the main peak of the speed  $Co(f_{\text{high}})$  and the low-frequency maximum  $Co(f_{\text{low}})$ .

The results of processing of all series of observations are shown in Fig. 13 and include the dependencies on the enhancement factor of:

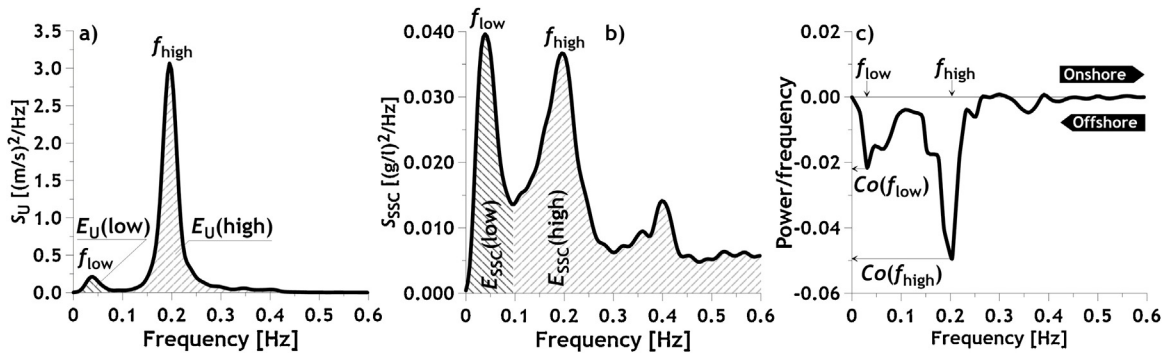


**Figure 12** Autospectra  $U$ -velocity components (a) and suspended sediment concentrations (b), with their cospectrum (c). Initial waves parameters:  $h_s = 1.2$  m,  $f_m = 0.2$  Hz,  $\gamma = 8.0$ .

- ratios of energies of low and high-frequency oscillations of water velocity (Fig. 13a);
- ratios of energies of low and high-frequency oscillations of near bottom suspended sediment concentrations (Fig. 13b);
- ratios of absolute cospectra values at low and high frequencies (Fig. 13c);
- values of cospectra at high frequencies (Fig. 13d).

Note that the enhancement factor in Fig. 13 is not the initial but the really observed one, calculated in the measuring point.

As it follows from Fig. 13a, with the parameter  $\gamma$  increases, the ratio  $E_U(\text{low})/E_U(\text{high})$  diminishes, the more intense the greater the significant wave height is. In case of a narrow spectrum (large values of  $\gamma$ ), the energy of the low-frequency oscillations of the  $E_U(\text{low})$  velocity is 5–6% of the

energy of the high-frequency components of the  $E_U(\text{high})$ , with the ratio practically independent of the values of  $h_s$  of the passing wave. In general, with increasing  $\gamma$ , the main energy of the flow velocity oscillations is concentrated in the high frequency range.

The pattern of suspension of the bottom material is influenced by a variety of hydro- and lithodynamic factors. For this reason, the dependence of the relation  $E_{SSC}(\text{low})/E_{SSC}(\text{high})$  on the enhancement factor cannot be unambiguous. With a relatively weak wave ( $h_s = 0.8$  m), the  $E_{SSC}(\text{low})/E_{SSC}(\text{high})$  ratio is fairly stable irrespective of the enhancement factor (Fig. 13b). With an increase in both the enhancement factor and the significant wave heights, the contribution of the low-frequency oscillations associated with the group structure of the waves decreases, and for  $\gamma > 5$  the energy of the low-frequency oscillations is 30–50% of the oscillation energy of the high-frequency range. We also

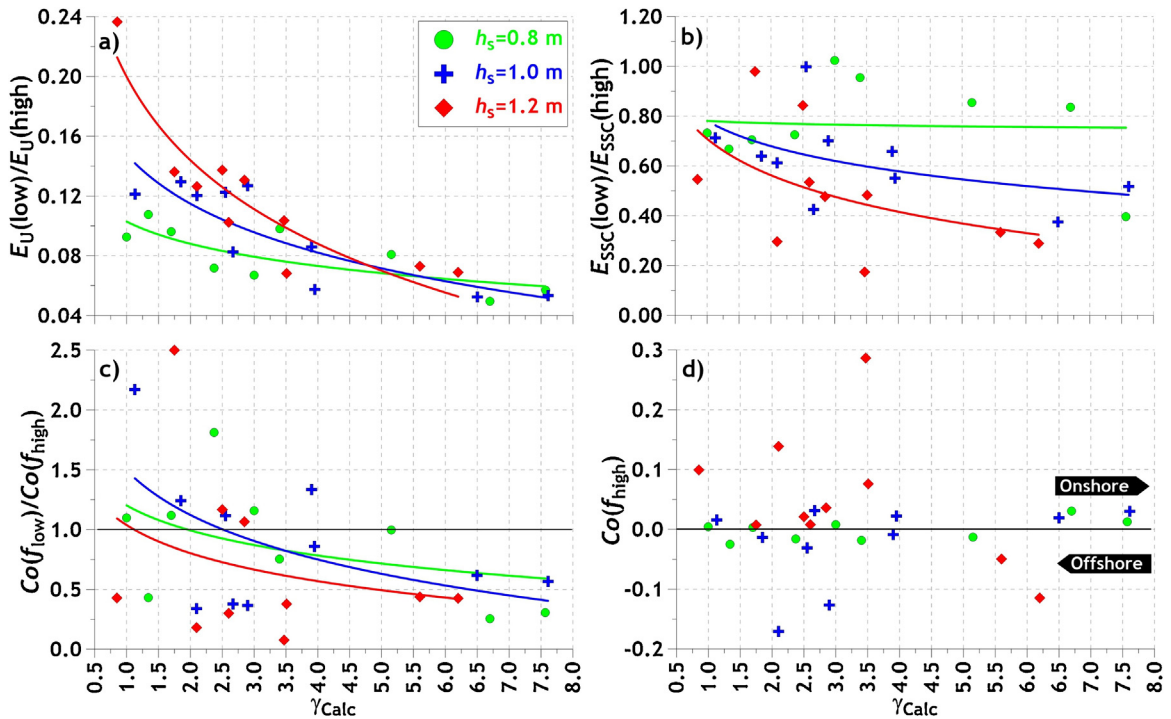


**Figure 13** Interrelation of spectral characteristics of synchronous velocity and concentration series with enhancement factors of the surface wave spectrum.

note that regardless of the magnitude of the significant wave heights, for  $\gamma < 3.5$  the oscillation energy of concentration fluctuations at low and high frequencies can be comparable ( $E_{SSC}(\text{low})/E_{SSC}(\text{high}) \sim 1$ ).

For  $\gamma < 5$ , the maximum mutual energy of the synchronous oscillations of the velocity and concentration series can be manifested at both low and high frequencies (Fig. 13c). This is evidenced by the ratio  $Co(f_{\text{low}})/Co(f_{\text{high}})$ , which can be either larger or smaller than 1. The dominance of synchronous oscillations in the region of the main maximum of the spectrum is noticeable for  $\gamma > 5$ , with  $Co(f_{\text{low}})/Co(f_{\text{high}}) \sim 0.5$ .

As already noted, the sign of the cospectrum of the flow velocity and concentrations of suspended sediment series determines the direction of transport of the bottom material. For all series of observations, low-frequency oscillations associated with the group structure of waves have a negative sign of the cospectra and thus contribute to the movement of sand from the shore. For oscillations related to the region of the main maximum of the spectrum, no one-to-one dependencies of the sign of the cospectrum on the enhancement factor were observed (Fig. 13d). Obviously, this may be due to the peculiarities of the formation of the bottom surface local microrelief in each particular case.

Thus, for equal integral wave parameters (wave height and period), the features of the spectral structure of surface waves determine the dominance of certain physical scales (of single waves or groups) in suspension processes. As the enhancement factor increases, the vibration energy of the concentration fluctuations at low frequencies decreases, and the energy of the suspension is thus concentrated in the region of the main maximum of the wave spectrum.

## 4. Conclusions

To analyze the influence of wave energy frequency distribution on the dynamics of the sea-bottom material suspension was the main objective of our research. We found differences in the responses of the eroded sea-bottom to external disturbances presented by irregular surface waves with constant integral characteristics (significant wave height and peak wave period) and variable frequency distribution of the wave energy.

It is worth mentioning that the conducted experiment can hardly be called perfect. Ideally, each series of experiments should be implemented under the same conditions: an even initial bottom and equal depths. In reality, these conditions are practically not feasible. The preliminary blank run of surface waves for, let us say, half an hour, could correct the situation to some extent, but this would require additional resources which was beyond our project.

We posted a simple question: “Does the spectral composition of the wave (with constant wave energy) influence the regularities of suspension?” As follows from the results of the experiment, the answer is rather positive.

We conclude that if the integral characteristics of irregular surface waves are the same ( $h_s, f_m = \text{const}$ ) the wave forcing applied to the sand bottom is determined precisely by the frequency distribution of the wave energy. Wave energy concentration within the spectrum maximum frequency band facilitates the transition from irregular to regular waves, and generally to the regular dynamic forcing

applied to the sand bottom. Physically, this leads to the realization of more stable external conditions for the development of the microforms of the sea-bottom topography.

The results presented here are not final but they show that further studies should be related to the analysis of the influence of frequency distribution of surface wave energy on the dynamics of sea-bottom material.

## Acknowledgments

This work was initialized by the Russian Science Foundation, project no. 14-17-00547. The processing of experimental data, used for this paper, was supported by the Russian Foundation for Basic Research, project no. 18-05-80035. The computer calculations were supported by the Russian Foundation for Basic Research (Projects no. 17-05-00183 and no. 16-45-230781). Analysis of the results was carried out within the framework of the program 0149-2019-0014.

We greatly thank Prof. Chris Vincent (School of Environmental Sciences, University of East Anglia) for fruitful discussions during preparations of this paper.

## References

- Davies, A.G., van Rijn, L.C., Damgaard, J.S., van de Graaff, J., Ribberink, J.S., 2002. Intercomparison of research and practical sand transport models. *Coast. Eng.* 46 (1), 1–23, [http://dx.doi.org/10.1016/S0378-3839\(02\)00042-X](http://dx.doi.org/10.1016/S0378-3839(02)00042-X).
- Divinsky, B.V., 2003. Results of wave measurements near Gelendzhik. In: Kosyan, R.D., Podymov, I.S., Pykhov, N.V. (Eds.), *Dynamic Processes in a Coastal Zone*. Moscow. 70–91, (in Russian).
- Divinsky, B.V., Kos'yan, R.D., Gruene, J., 2014. Influence of the wave spectrum form on the bottom sediment dynamics. *Oceanologia* 54 (2), 132–143, <http://dx.doi.org/10.1134/S0001437014020052>.
- Dohmen-Janssen, C.M., McLean, S.R., Ribberink, J.S., Hanes, D.M., Vincent, C.E., 2000. Sheet flow and suspension under wave groups in a Large Wave Flume (SISTEX99). *Eos, Transactions, AGU Fall meeting Suppl.* 81 (48), F642.
- Grüne, J., Kos'yan, R., Oumeraci, H., Podymov, I., Schmidt-Koppenhagen, R., Vincent, C.E., 2007. Large-scale laboratory modeling of suspended sand concentration fluctuations under irregular waves. *Coastal Sediments 07*. ASCE, New Orleans, 248–258, [http://dx.doi.org/10.1061/40926\(239\)19](http://dx.doi.org/10.1061/40926(239)19).
- Hasselmann, K., Barnett, T.P., Bouws, E., Carlson, H., Cartwright, D. E., Enke, K., Ewing, J.A., Gienapp, H., Hasselmann, D.E., Kruseman, P., Meerburg, A., Müller, P., Olbers, D.J., Richter, K., Sell, W., Walden, H., 1973. Measurements of wind-wave growth and swell decay during the Joint North Sea Wave Project (JONSWAP). In: *Ergänzungsheft zur Deutschen Hydrographischen Zeitschrift, A* (8°), No. 12. Deutsches Hydrograph. Inst., Hamburg, 96 pp.
- Kos'yan, R., Grüne, J., Divinskiy, B., Podymov, I., Vincent, C., Ahmari, A., Oumeraci, H., 2010. The dependence of suspended sand concentration on the degree of storm development. *Coast. Eng. Proc.* 32, 8 pp., <http://dx.doi.org/10.9753/icce.v32.sediment.19>.
- Moate, B.D., Thorne, P.D., 2011. Interpreting acoustic backscatter from suspended sediments of different and mixed mineralogical composition. *Cont. Shelf. Res.* 46 (1), 67–82, <http://dx.doi.org/10.1016/j.csr.2011.10.007>.
- Thorne, P.D., Hanes, D.M., 2002. A review of acoustic measurement of small-scale sediment processes. *Cont. Shelf. Res.* 22 (4), 603–632, [http://dx.doi.org/10.1016/S0278-4343\(01\)00101-7](http://dx.doi.org/10.1016/S0278-4343(01)00101-7).

- Thorne, P.D., Meral, R., 2008. Formulations for the scattering properties of suspended sandy sediments for use in the application of acoustics to sediment transport processes. *Cont. Shelf. Res.* 28 (2), 309–317, <http://dx.doi.org/10.1016/j.csr.2007.08.002>.
- Thorne, P.D., Vincent, C.E., Hardcastle, P.J., Rehman, S., Pearson, N., 1991. Measuring suspended sediment concentrations using acoustic backscatter devices. *Mar. Geol.* 98 (1), 7–16, [http://dx.doi.org/10.1016/0025-3227\(91\)90031-X](http://dx.doi.org/10.1016/0025-3227(91)90031-X).
- Vincent, C.E., Hanes, D.M., 2002. The accumulation and decay of nearbed suspended sand concentration due to waves and wave groups. *Cont. Shelf. Res.* 22 (14), 1987–2000, [http://dx.doi.org/10.1016/S0278-4343\(02\)00051-1](http://dx.doi.org/10.1016/S0278-4343(02)00051-1).